

Coordination-Driven Self-Assembly of Cyclometalated Iridium Squares Using Linear Aromatic Diisocyanides

Morris E. Olumba, Hanah Na, Alan E. Friedman, and Thomas S. Teets*

Cite This: *Inorg. Chem.* 2021, 60, 5898–5907

Read Online

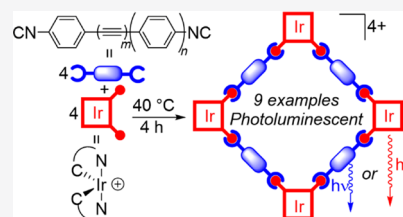
ACCESS |

Metrics & More

Article Recommendations

Supporting Information

ABSTRACT: Here, we demonstrate facile $[4 + 4]$ coordination-driven self-assembly of cyclometalated iridium(III) using linear aryldiisocyanide bridging ligands (BLs). A family of nine new $[\text{Ir}(\text{C}^{\wedge}\text{N})_2(\mu\text{-BL})_4]^{4+}$ coordination cages is described, where $\text{C}^{\wedge}\text{N}$ is the cyclometalating ligand—2-phenylpyridine (ppy), 2-phenylbenzothiazole (bt), or 1-phenylisoquinoline (piq)—and BL is the diisocyanide BL, with varying spacer lengths between the isocyanide binding sites. These supramolecular coordination compounds are prepared via a one-pot synthesis, with isolated yields of 40–83%. ^1H NMR spectroscopy confirms the selective isolation of a single product, which is affirmed to be the M_4L_4 square by high-resolution mass spectrometry. Detailed photophysical studies were carried out to reveal the nature of the luminescent triplet states in these complexes. In most cases, phosphorescence arises from the $[\text{Ir}(\text{C}^{\wedge}\text{N})_2]^+$ nodes, with the emission color determined by the cyclometalating ligand. However, in two cases, the lowest-energy triplet state resides on the aromatic core of the BL, and weak phosphorescence from that state is observed. This work shows that aromatic diisocyanide ligands enable coordination-driven assembly of inert iridium(III) nodes under mild conditions, producing supramolecular coordination complexes with desirable photophysical properties.



INTRODUCTION

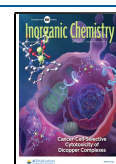
The synthesis of photoactive two- and three-dimensional polynuclear metallocage assemblies has become a particular area of focus in photochemistry, owing to the unique excited-state dynamics of these systems which provide insights into excited-state energy and charge-transfer phenomena.^{1,2} Some of the most well-studied and characterized complexes of this nature are ruthenium-, rhenium-, and platinum-based assemblies with polypyridyl or metalloporphyrin bridging ligands (BLs).^{3–6} Platinum coordination cages have become especially popular for their use as molecular sensors, while ruthenium, rhenium, and palladium coordination cages have seen use in photocatalytic applications.^{6–10} Comparatively few examples of iridium coordination assemblies have been reported, despite the robust luminescence properties of many iridium complexes.^{11–14} One factor contributing to this lack of development is the significant substitutional inertness of iridium(III), which can necessitate high temperatures and long reaction times for the assembly of cages with iridium(III) building blocks.¹⁵ However, due to the *trans*-effect labilization brought on by the cyclometalated aryl groups, ligand substitution chemistry on bis-cyclometalated iridium complexes can be readily achieved, and they have the potential to be versatile building blocks for luminescent supramolecular assemblies.

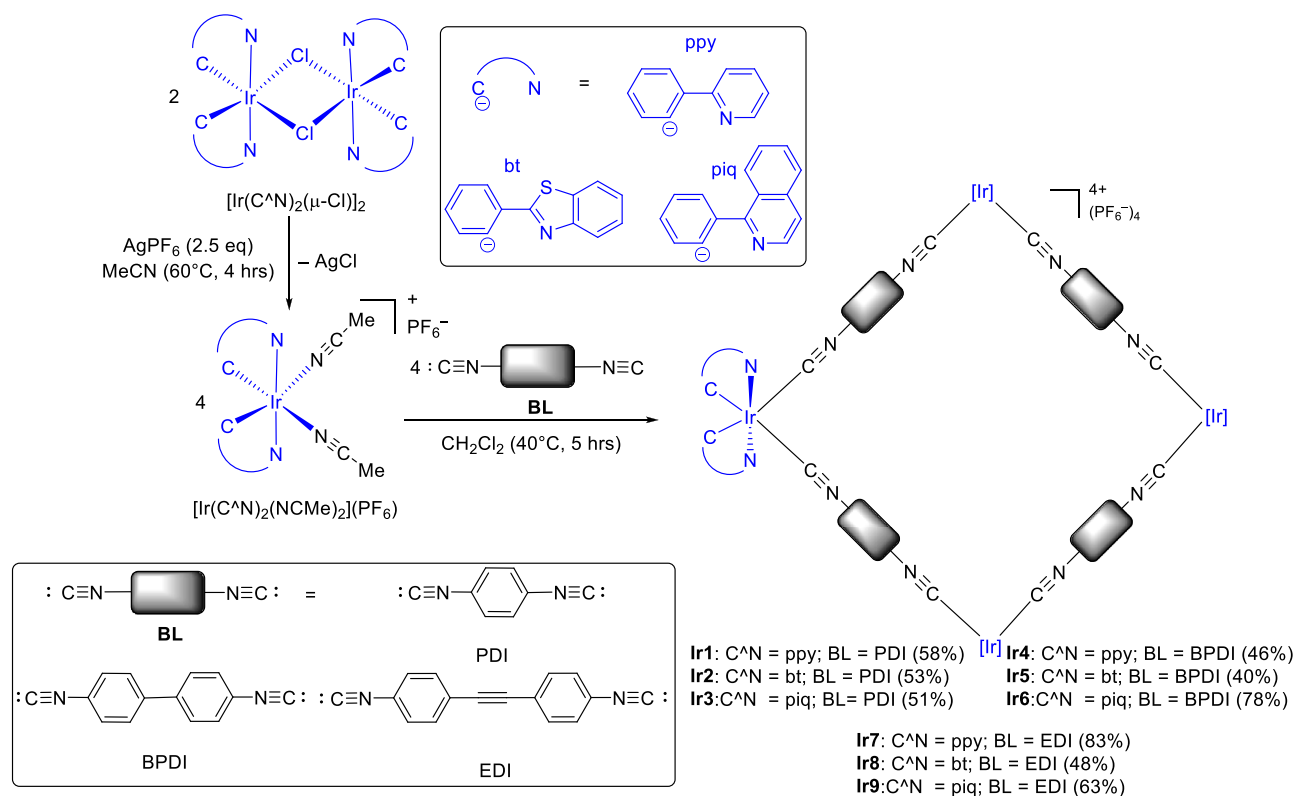
Arguably the most efficient synthetic approach for supramolecular photoactive cages or metallacycles is coordination-driven self-assembly, in which molecules organize into ordered, well-defined structures as a consequence of directional metal–ligand bond formation.⁸ Coordination-driven self-assembly

enables the facile assembly of complex frameworks with predictable geometries in high yields. The structures that are formed by this route are often categorized using the “ M_xL_y ” notation, where x is the number of metal nodes and y is the number of BLs that span these nodes. Several luminescent platinum assemblies have been prepared via this methodology, largely due to the ease of self-assembly of square-planar platinum complexes.^{8,16} Ruthenium and rhenium have also been used as the luminescent nodes in several self-assembly schemes.^{3,6,17,18} Iridium(III) coordination cages have been previously reported, including some with half-sandwich iridium building blocks that were not reported to be photoluminescent or photochemically active.^{19,20} Recently, there have been reports of coordination-driven self-assembly of cyclometalated iridium(III) coordination cages, where the building blocks are known to exhibit efficient, highly tunable phosphorescence. Using a strategy that had previously been adopted to prepare square tetranuclear assemblies of several other metals,^{21–24} Baranoff et al. prepared luminescent tetranuclear M_4L_4 complexes where four bis-cyclometalated iridium fragments were bridged by cyanide ligands.¹¹ Chepelin et al. accessed enantiopure three-dimensional hexanuclear M_6L_4 capsules

Received: January 30, 2021

Published: March 30, 2021



Scheme 1. Synthesis of Cyclometalated Iridium Squares via Coordination-Driven Self-Assembly^a

^aIsolated yields are shown in parentheses.

where the bis-cyclometalated iridium nodes were bridged by 1,3,5-tricyanobenzene linkers, studied the photoluminescence of these cages, and demonstrated host–guest chemistry of noncoordinating anions inside the cationic hexairidium cage.¹² Most recently, Oldknow et al. reported a three-dimensional M_3L_2 cage using a chiral tripodal cyclotriguaiacylene-derived M_3L_2 cage using a chiral tripodal cyclotriguaiacylene-derived BL, functionalized with photoisomerizable azo-aromatic linkers.¹³ These cages all make use of the well-studied cyano and pyridyl building blocks as the BL between the cyclometalated iridium metal centers.

In consideration of the above examples, there is room to expand the coordination-driven self-assembly of cyclometalated iridium(III). Here, we introduce linear bidentate aryl isocyanides as bridging ligands for self-assembled M_4L_4 cyclometalated iridium squares, varying the cyclometalating ligand on iridium and the length of the bridging ligand. The cyclometalating ligands were chosen to vary the triplet energy of the bis-cyclometalated iridium node, descending in the order 2-phenylpyridine (ppy), 2-phenylbenzothiazole (bt), and 1-phenylisoquinoline (piq). Linear diisocyanides of the type described here have been used in surface chemistry^{25–27} and as bridging ligands for multimetallic structures,^{28–32} but their application in coordination-driven self-assembly is underexplored. We used three different linear aryl diisocyanides with varying spacer lengths in this study. Commercially available 1,4-phenylene diisocyanide (PDI) and the known compound 4,4'-diisocyanato-1,1'-biphenyl (BPDI) have been previously described,^{25–32} and we also introduce here the new ligand 1,1'-(1,2-ethynediyl)bis(4-isocyanobenzene) (EDI) with a longer π -conjugated linker between the two isocyanides. Our hypothesis is that bridging isocyanides offer several potential synthetic advantages in the assembly of polynuclear complexes

with cyclometalated iridium building blocks. The nitrile- and pyridine-based bridging ligands that are ubiquitous in coordination-driven self-assembly often require high temperatures and long reaction times to assemble substitutionally inert metal nodes,^{12,33} but isocyanides are stronger σ -donors and thus should assemble more rapidly and with milder conditions. Moreover, aryl isocyanide moieties are easily installed in two steps from aniline precursors,³⁴ so it should be possible to prepare a large variety of directionally oriented polynucleating ligands to template a wide range of structures. Beyond these synthetic advantages, previous works from our group have demonstrated some beneficial photophysical consequences when aryl isocyanides are paired with cyclometalated iridium. In a series of mononuclear bis-cyclometalated iridium complexes with aryl isocyanide ancillary ligands, we showed that the π -acidic isocyanides stabilize the iridium-centered $d\pi$ HOMOs, which results in greater redox stability and blue-shifted photoluminescence relative to many other cyclometalated iridium complexes.^{35–37} High quantum yields and long lifetimes, on the order of 10^{-5} s, were noted for the blue- and green-phosphorescent members of these series.

The work described here demonstrates these aforementioned synthetic benefits, where coordination-driven self-assembly of labile cyclometalated precursors with linear bidentate aryl isocyanides enables rapid preparation of M_4L_4 squares under mild reaction conditions. The M_4L_4 squares are characterized by NMR and high-resolution mass spectrometry, which evince clean, high-yielding formation of the products. The photophysical properties of the tetranuclear complexes are all described, with a combination of UV–vis absorption and steady-state and time-resolved photoluminescence measurements providing insights into the nature of the excited states in

these compounds. The isocyanide can have photophysical consequences, with the longer, more conjugated bridging ligands allowing energy transfer from the bis-cyclometalated iridium-localized triplet state to a bridging-ligand-centered state, which can influence the observed photoluminescence. This work shows that linear aryl diisocyanides are very effective bridging ligands for [4 + 4] self-assembly of luminescent tetranuclear cyclometalated iridium complexes. The synthetic advances and photophysical properties described here support the continued use of this ligand class in the design of photoactive constructs for fundamental studies of molecular photophysics and applications in optoelectronics and sensing.

RESULTS AND DISCUSSION

Synthesis and Characterization. The three-step synthetic procedure for the new complexes described in this report is summarized in Scheme 1. Synthesis begins with the ubiquitous chloride-bridged dimers $[\text{Ir}(\text{C}^{\wedge}\text{N})_2(\mu\text{-Cl})_2]_2$ ($\text{C}^{\wedge}\text{N}$ = cyclometalating ligand), prepared by refluxing $\text{IrCl}_3 \cdot n\text{H}_2\text{O}$ with 2.5 equivalents cyclometalating ligand following the known Nonoyama procedure.³⁸ The chloro-bridged dimer is subsequently cleaved by refluxing the dimer with 2.5 equivalents silver hexafluorophosphate (AgPF_6) in acetonitrile at 60 °C.^{39,40} This forms a cationic mononuclear iridium bis-acetonitrile complex $[\text{Ir}(\text{C}^{\wedge}\text{N})_2(\text{NCMe})_2](\text{PF}_6)$, a synthon previously used to construct cationic monometallic cyclometalated iridium complexes.⁴¹ The $[\text{Ir}(\text{C}^{\wedge}\text{N})_2(\text{NCMe})_2](\text{PF}_6)$ intermediate is refluxed in a 1:1 ratio with one of the linear aromatic diisocyanides in dichloromethane at 40 °C for 5 h, which produces the M_4L_4 squares. Purification of all complexes was achieved by precipitation of the complex from dichloromethane with diethyl ether. Three different cyclometalating ligands ($\text{C}^{\wedge}\text{N}$) and three different diisocyanide BLs were used, producing nine complexes (**Ir1–Ir9**) using the same general route, with moderate to good isolated yields ranging between 40 and 83%. Crude NMR spectra indicate that the M_4L_4 products are the major products formed, so in cases where the isolated yield is modest, there was some product loss during the precipitation step. The linear bridging diisocyanide ligands (BPDI and EDI) were synthesized using a known two-step procedure.³⁴ A linear arylidiane precursor is formylated using acetic anhydride and formic acid at 0 °C in tetrahydrofuran, which forms acetic formic anhydride in situ as the formylating agent. The resulting formylamide is then dehydrated with phosphoryl chloride and diisopropyl amine to yield the linear diisocyanides.

The synthesized complexes were characterized by ^1H NMR, infrared (IR) spectroscopy, and mass spectrometry. The ^1H NMR spectra are reproduced in the Supporting Information. Figures S1–S3 show the spectra of the mononuclear acetonitrile-bound precursors, and Figures S4–S12 show the spectra for the M_4L_4 squares **Ir1–Ir9**. NMR spectra of the squares are consistent with the isolation of a single product in each case, and the number of aromatic peaks and their integration suggest localized C_2 symmetry at each iridium node. Comparison of the NMR spectra of **Ir1–Ir9** with those of the acetonitrile precursors in the same solvent, as shown in Figures S13–S15, allows us to assign which peaks originate from the $\text{C}^{\wedge}\text{N}$ ligands and which come from the BLs. ^1H NMR peaks associated with the BLs typically overlap with peaks from the $\text{C}^{\wedge}\text{N}$ ligands and thus are difficult to conclusively identify, but comparison with the free ligand spectra (Figures S16 and S18) suggests that the *ortho* C–H resonances in the BLs only

exhibit subtle shifts when coordinated in the squares. The self-assembled products **Ir1–Ir9** were recalcitrant to forming single crystals, but high-resolution electrospray ionization mass spectrometry (ESI-MS) demonstrates selective formation of the [4 + 4] M_4L_4 squares. Intact molecular ion peaks were observed in each complex, the most intense being the $[\text{M} - 3\text{PF}_6]^{3+}$ ion observed in all nine complexes, with representative examples shown in Figure 1 for the BL = PDI series, **Ir1–Ir3**. Mass spectrometry data for all nine complexes are shown in Supporting Information, Figures S20–S28. In **Ir1–Ir6**, the $[\text{M} - 2\text{PF}_6]^{2+}$ ion is also resolved, in addition to the 3+ ion. There is a good match between the observed and theoretical m/z

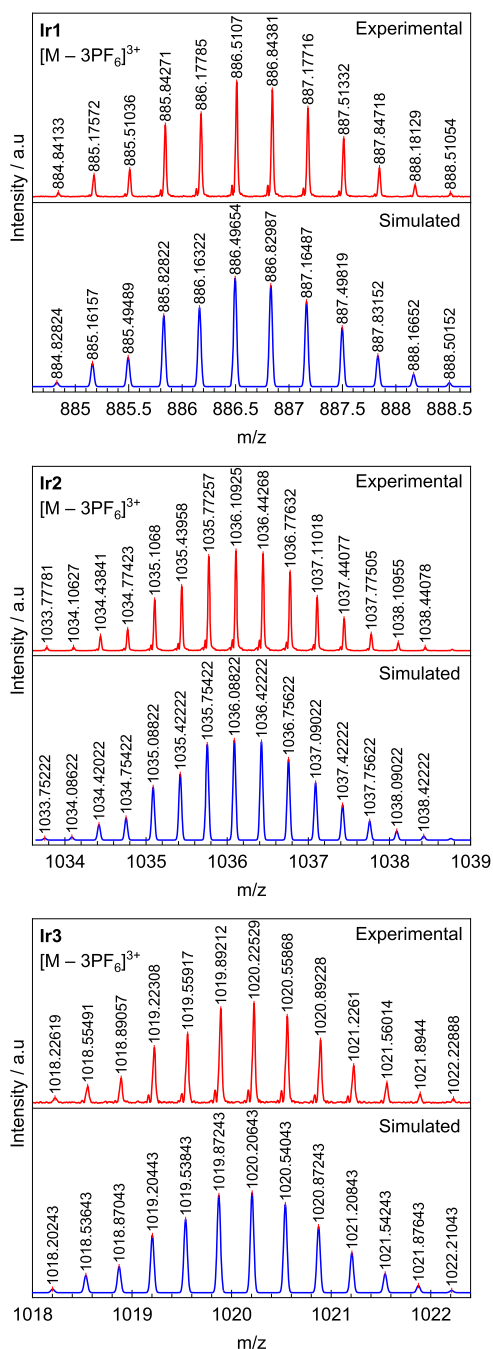


Figure 1. ESI-MS of **Ir1–Ir3**, with each plot showing the experimental (top) and simulated (bottom) isotopologue pattern for the $[\text{M} - 3\text{PF}_6]^{3+}$ fragment. Peak positions are marked.

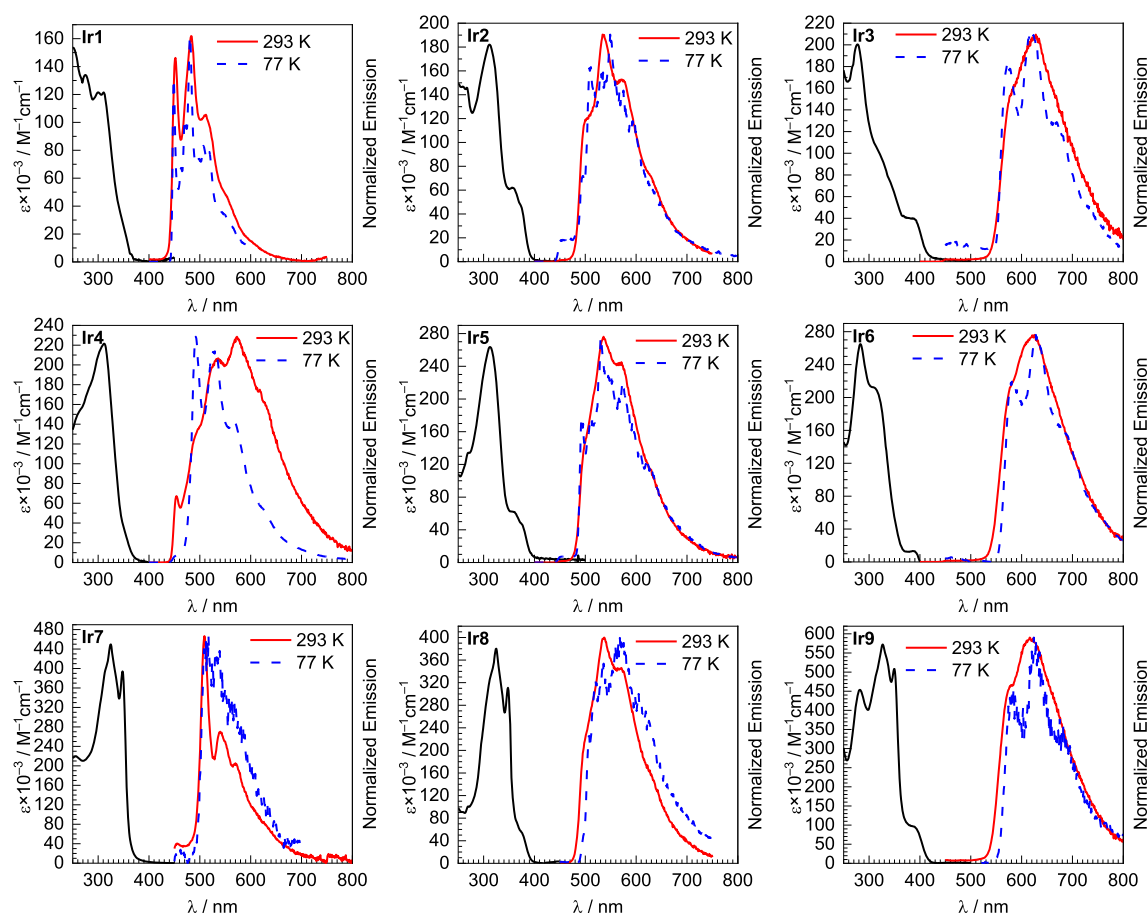


Figure 2. Overlaid UV-vis absorption spectra (black solid lines) in CH_2Cl_2 at 293 K and photoluminescence spectra in CH_2Cl_2 at 293 K (red solid lines) and 1:3 CH_2Cl_2 /toluene at 77 K (blue dashed lines) for complexes **Ir1–Ir9**.

Table 1. Summary of the Photophysical Properties of Complexes **Ir1–Ir9**

	UV-vis absorption λ/nm ($\epsilon \times 10^{-3}/\text{M}^{-1}\text{cm}^{-1}$)	photoluminescence $\lambda_{\text{max}}/\text{nm}$		Φ_{PL}	$\tau/\mu\text{s}$
		CH_2Cl_2 at 293 K	CH_2Cl_2 /toluene at 77 K		
Ir1	251 (153), 275 (134), 311 (121)	452, 483, 512	449, 481, 507	0.018	10 ^b
Ir2	267 (146), 313 (182), 356 (62)	500, 534, 572	508, 549, 575	0.29	15 ^b
Ir3	277 (200), 388 (40)	628	574, 621, 669 (sh)	0.050	17 ^b
Ir4	312 (222)	454, 492, 533, 573	492, 532, 568	0.012	44
Ir5	312 (264), 359 (62)	499, 536, 571	493, 530, 573, 622	0.14	22
Ir6	283 (265), 311 (212), 386 (13)	625	582, 628	0.048	12
Ir7	325 (450), 348 (394)	509, 540, 572	517	N.D. ^a	15 ^b
Ir8	325 (380), 348 (311), 373 (57)	487, 537, 570	534, 572, 605	0.11	20
Ir9	282 (454), 327 (572), 350 (508), 389 (96)	576, 616	581, 624, 675	0.077	10
$[\text{Ir}(\text{ppy})_2(\text{CN}^{\text{dmp}})_2]\text{PF}_6$ ³⁵	258 (60), 310 (sh,16), 343 (9)	454, 486, 512	449, 481, 509, 529 (sh)	0.24	30
$[\text{Ir}(\text{bt})_2(\text{CN}^{\text{dmp}})_2]\text{PF}_6$ ³⁵	315 (40), 361 (20), 376 (sh,16)	500, 536, 576	497, 535, 580, 631	0.33	36
$[\text{Ir}(\text{piq})_2(\text{CN}^{\text{dmp}})(\text{py})]\text{PF}_6$ ⁴²	286 (52), 354 (19), 406 (9.6)	587 (sh), 625	577, 625, 683	0.096	6.0

^aPhotoluminescence is too weak at room-temperature for an accurate determination. Estimated upper limit is 0.001. ^bEmission decay trace was the best fit as a biexponential. The reported lifetime is a weighted average of the two time constants. The last three rows include data for the mononuclear bis-cyclometalated iridium complexes $[\text{Ir}(\text{C}^{\wedge}\text{N})_2(\text{CN}^{\text{dmp}})_2]\text{PF}_6$ ($\text{C}^{\wedge}\text{N}$ = ppy or bt, CN^{dmp} = 2,6-dimethylphenyl isocyanide) and $[\text{Ir}(\text{piq})_2(\text{CN}^{\text{dmp}})(\text{py})]\text{PF}_6$ (py = pyridine), previously published by our group.^{35,42}

peak positions and isotopologue distribution patterns for each molecular ion peak. IR spectra, as shown in Figures S29–S40 of Supporting Information for the three free ligands (PDI, BPDI, and EDI) and **Ir1–Ir9**, are consistent with the formulated structures. Assuming a localized D_{4h} symmetry environment for the M_4L_4 squares, ignoring the influence of

the $\text{C}^{\wedge}\text{N}$ ligands on each iridium, there should be two IR-active E_u stretching modes, and for all complexes, there is a strong $\tilde{\nu}_{\text{CN}}$ stretching band observed, along with a second band as a shoulder at slightly higher frequency. The strongest $\tilde{\nu}_{\text{CN}}$ band occurs between 2126 and 2144 cm^{-1} in the nine Ir squares, slightly higher frequency than the same band in the

free ligands (2125, 2124, and 2125 cm^{-1} for PDI, BPDI, and EDI, respectively).

Photophysical Properties. The UV–vis absorption and photoluminescence emission spectra of complexes **Ir1–Ir9** are shown in Figure 2. The UV–vis absorption spectra were recorded at 293 K in CH_2Cl_2 , and photoluminescence was recorded both at 293 K in CH_2Cl_2 and at 77 K in 1:3 CH_2Cl_2 /toluene glass. All photophysical data are summarized in Table 1. The absorption spectra of phenylene and biphenylene-bridged **Ir1–Ir6** show two main features, falling in line with several other characterized bis-cyclometalated iridium complexes with aryl isocyanide ancillary ligands.^{35,36,42} In the UV ($\lambda < 350$ nm), there are intense absorption bands occurring at similar wavelengths for all six of these compounds; these are assigned to localized, ligand-centered (^1LC or $^1\pi \rightarrow \pi^*$) transitions on the cyclometalating and BLs. In addition, a less intense, lower-energy shoulder is resolved in the spectra of the complexes with $\text{C}^{\wedge}\text{N} = \text{bt}$ and piq , assigned to a metal-to-ligand-charge-transfer ($^1\text{MLCT}$) excitation. This band is presumably obscured in the $\text{C}^{\wedge}\text{N} = \text{ppy}$ complexes (**Ir1** and **Ir4**) by the more intense ^1LC bands, but it occurs at ~ 360 nm when $\text{C}^{\wedge}\text{N} = \text{bt}$ (**Ir2** and **Ir5**) and at ~ 390 nm when $\text{C}^{\wedge}\text{N} = \text{piq}$ (**Ir3** and **Ir6**). Whereas the positions of these bands are quite similar to mononuclear isocyanide-ligated cyclometalated iridium complexes,^{35,36,42} the molar absorptivity values are ca. 4 \times larger, as expected given the tetranuclear nature of these complexes. The UV–vis absorption spectra of the diphenylethynyl-spaced complexes **Ir7–Ir9** (BL = EDI) are markedly different, dominated in the UV by intense transitions originating from the BL. All three BL = EDI complexes have nearly identical and very intense bands at ca. 325 and 350 nm, assigned to $^1\pi \rightarrow \pi^*$ transitions on the EDI ligand, with the ca. 2200 cm^{-1} spacing suggestive of a vibronic progression involving the alkyne $\text{C}\equiv\text{C}$ stretching motion. Consistent with this assignment, the spectrum of free EDI (Figure S50) shows two similarly spaced sharp bands, blue-shifted by ca. 2500 cm^{-1} in the free ligand relative to the M_4L_4 squares. These bands are considerably more intense than the ligand-localized transitions in **Ir1–Ir6**, by a factor of 1.5 or more. In **Ir8** ($\text{C}^{\wedge}\text{N} = \text{bt}$) and **Ir9** ($\text{C}^{\wedge}\text{N} = \text{piq}$), $^1\text{MLCT}$ transitions at lower energy are resolved, occurring at very similar wavelengths as the corresponding bands in the other complexes with the same cyclometalating ligands.

The photoluminescence spectra of **Ir1–Ir9** are also displayed in Figure 2. For the complexes with $\text{C}^{\wedge}\text{N} = \text{bt}$ and piq , which respectively luminesce in the green and red regions, the photoluminescence profiles are very similar for a given $\text{C}^{\wedge}\text{N}$ ligand, and strongly resemble mononuclear cationic bis-cyclometalated iridium complexes with similar coordination environments. In these cases, phosphorescence arises from a triplet state centered on a $[\text{Ir}(\text{C}^{\wedge}\text{N})_2]^+$ fragment of mixed $\text{C}^{\wedge}\text{N} ^3\text{LC}$ and $^3\text{MLCT}$ character, as is typical for cyclometalated iridium complexes.⁴³ In particular, we have previously studied several mononuclear $[\text{Ir}(\text{bt})_2(\text{CNAr})_2]^+$ complexes,^{35,36} which exhibit photoluminescence profiles nearly identical to the $[\text{Ir}(\text{bt})_2(\mu\text{-BL})]_4^{4+}$ squares presented here (**Ir2**, **Ir5**, and **Ir8**). The peak emission wavelengths of the M_4L_4 squares and their mononuclear analogues fall within 4 nm (140 cm^{-1}) of one another, and in all cases, there is a discernible vibronic structure at room temperature with three maxima observed. There is some effect of the BLs on the photoluminescence quantum yield and lifetime. The lifetimes of **Ir2**, **Ir5**, and **Ir8** are similar to one another and slightly shorter than typical

lifetimes for mononuclear bis-isocyanide complexes with the same $\text{C}^{\wedge}\text{N}$ ligand. For complex **Ir2**, which uses the phenylene-spaced bridging isocyanide PDI, the photoluminescence quantum yield (Φ_{PL}) is 0.29, almost identical to typical mononuclear $[\text{Ir}(\text{bt})_2(\text{CNAr})_2]^+$ complexes. However, the Φ_{PL} value drops slightly with the longer, more conjugated BLs, BPDI (**Ir5**, $\Phi_{\text{PL}} = 0.14$) and EDI (**Ir8**, $\Phi_{\text{PL}} = 0.11$). As discussed in detail below, we believe this decrease is due to the interference of nearby weakly luminescent triplet states centered on the ^3BL , which are thermally populated at room temperature. Although we do not have a direct bis-isocyanide analogue to compare to, we do note that the photoluminescence spectra of piq squares **Ir3**, **Ir6**, and **Ir9**, in addition to strongly resembling one another, are quite similar to cationic $[\text{Ir}(\text{piq})_2(\text{CNAr})_2]^+$ complexes we have previously described.⁴² In the piq series, there is no systematic dependence of the lifetime or quantum yield on the BL. Quantum yields are modest, as is typically the case for cationic red-phosphorescent complexes, and the lifetimes of all three are similar, suggesting that in the piq series, the bridging-ligand triplet states do not interfere. Photoluminescence spectra were also collected at 77 K in rigid solvent glass, as shown in Figure 2, and in all cases, there is a more pronounced vibronic structure at low temperature but minimal shifts in peak wavelengths, consistent with the T_1 state being predominately $\text{C}^{\wedge}\text{N} ^3\text{LC}$. To summarize, for the M_4L_4 squares with $\text{C}^{\wedge}\text{N} = \text{bt}$ or piq , the photoluminescence arises from a mixed $^3\text{LC}/^3\text{MLCT}$ state centered on one of the $[\text{Ir}(\text{C}^{\wedge}\text{N})_2]^+$ nodes, and the photophysical properties of the nodes are retained upon assembling the cyclometalated iridium fragments into a metalacyclic structure.

In contrast, for the $\text{C}^{\wedge}\text{N} = \text{ppy}$ series (**Ir1**, **Ir4**, and **Ir7**), the photoluminescence behavior is strongly dependent on the bridging isocyanide ligand. To visualize the differences more clearly between these three complexes, their spectra at both 293 and 77 K are overlaid, as shown in Figure 3. In the phenylene-spaced $[\text{Ir}(\text{ppy})_2(\mu\text{-PDI})_2]_4^{4+}$ square (**Ir1**), the photoluminescence is in the blue–green region and strongly resembles mononuclear $[\text{Ir}(\text{ppy})_2(\text{CNAr})_2]^+$ complexes.³⁵ A sharp vibronic structure is noted, and the peak maxima in **Ir1** are within 3 nm (130 cm^{-1}) of the mononuclear analogues (see Table 1). That said, the quantum yield of **Ir1** is quite modest ($\Phi_{\text{PL}} = 0.018$), in contrast to the brightly luminescent mononuclear analogues ($\Phi_{\text{PL}} = 0.24\text{--}0.37$), and the lifetime of **Ir1** (10 μs) is more than a factor of 2 smaller. The photoluminescence spectra in **Ir4** (BL = BPDI) and **Ir7** (BL = EDI) are dramatically different, as shown in Figures 2 and 3. The spectra are significantly red-shifted from that of **Ir1**, again with the well-resolved vibronic structure and quantum yields that are modest (**Ir4**; $\Phi_{\text{PL}} = 0.012$) or negligible (**Ir7**; $\Phi_{\text{PL}} < 0.001$). Complex **Ir4** has the longest lifetime in the series at 44 μs , and despite its very weak photoluminescence, the lifetime of **Ir7** is also quite long at 15 μs . The spectra at 77 K are also distinct from one another, which provides further evidence that the three $\text{C}^{\wedge}\text{N} = \text{ppy}$ complexes all luminesce from different triplet states.

Although **Ir1** and all $\text{C}^{\wedge}\text{N} = \text{bt}$ and piq complexes clearly luminesce from the typical $[\text{Ir}(\text{C}^{\wedge}\text{N})_2]^+ ^3\text{LC}/^3\text{MLCT}$ state, we propose that the T_1 states in **Ir4** and **Ir7** are centered on the bridging isocyanide ligands, denoted here as ^3BL states. The free ligands BPDI and EDI are not luminescent at room temperature or at 77 K in transparent solvent glass. Thus, we do not have phosphorescence spectra of BPDI to compare to,

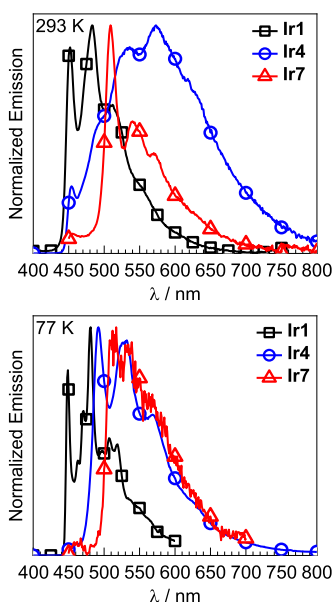


Figure 3. Overlaid emission spectra of C[^]N = ppy complexes **Ir1**, **Ir4**, and **Ir7**, recorded in CH₂Cl₂ at 293 K (top) and in 1:3 CH₂Cl₂/toluene at 77 K (bottom). Data are the same as that shown in Figure 2, showing these three complexes to illustrate the effect of the BL on their photoluminescence. Symbols were added to help distinguish the overlaid plots.

but the phosphorescence of the biphenyl core is well-studied.⁴⁴ As shown in Figure 4, the phosphorescence in **Ir4** bears a striking resemblance to that of biphenyl, with a similar profile and vibronic structure, albeit ca. 800 cm⁻¹ red-shifted on account of the isocyano groups, which are electron-withdrawing and extend the conjugation. Moreover, the longer

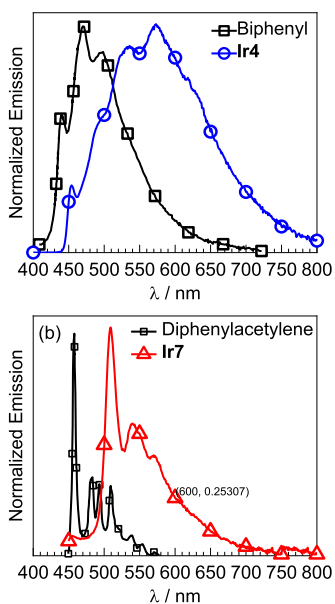


Figure 4. Overlaid spectra of (a) phosphorescence of biphenyl and **Ir4** and (b) phosphorescence of diphenylacetylene (recorded at 77 K) and **Ir7**. Symbols were added to help distinguish the overlaid plots. The spectrum for biphenyl is adapted with permission from ref 44. Copyright 2020 American Chemical Society. The spectrum for diphenylacetylene is adapted from ref 45. Copyright 2003 American Chemical Society.

lifetime in **Ir4**, compared to the other M₄L₄ squares, is consistent with luminescence arising from an aromatic triplet state on the BL. Similarly, while the EDI ligand also does not produce phosphorescence on its own, we can compare the phosphorescence of **Ir7** to that of the conjugated hydrocarbon core. As also shown in Figure 4, the phosphorescence of **Ir7** is similar to that of diphenylacetylene,⁴⁵ again with a significant red-shift (ca. 2000 cm⁻¹) brought on by the introduction of isocyano groups. The vibronic spacing of ca. 1100 cm⁻¹ in **Ir7** is consistent with totally symmetric modes within the diphenylacetylene core.⁴⁵ Thus, in **Ir4** and **Ir7**, the lowest-energy triplet state is centered on the aromatic BL and not on the [Ir(ppy)₂]⁺ node. This switching of phosphorescence from the normal C[^]N-centered ³LC/³MLCT state to the isocyanide ancillary ligand has been observed before in mononuclear complexes. In our own previous work, we showed that phosphorescence can originate from a naphthyl-centered triplet state in certain bis-cyclometalated iridium complexes with 2-naphthyl isocyanide ancillary ligands,³⁵ and Favale et al. have shown similar behavior in complexes with oligoaryl isocyanide ancillary ligands.⁴⁶

To summarize the photoluminescence properties of these compounds, Figure 5 shows qualitative energy-level diagrams for the complexes presented here. The UV-vis absorption

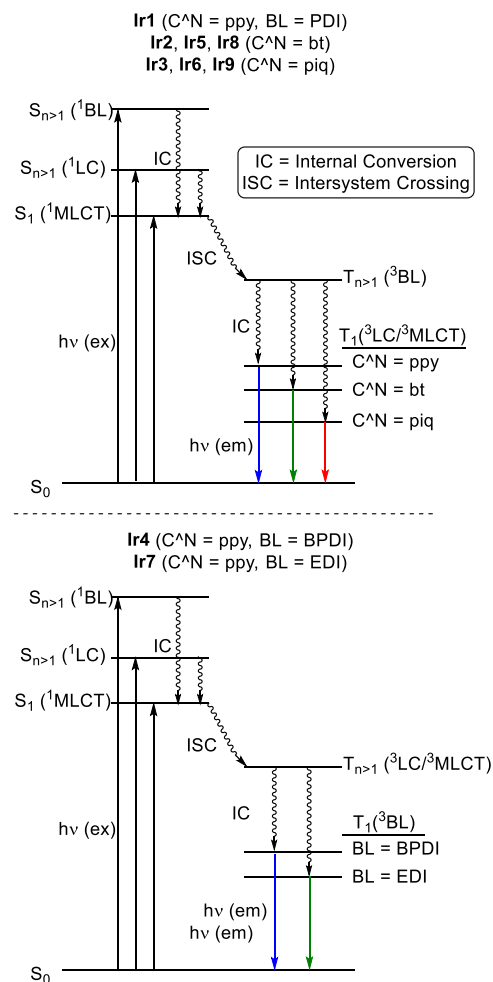


Figure 5. Qualitative excited-state energy-level diagram for M₄L₄ squares **Ir1–Ir9**. The top diagram pertains to **Ir1–Ir3**, **Ir5**, **Ir6**, **Ir8**, and **Ir9**. The bottom diagram pertains to **Ir4** and **Ir7**.

spectra of all compounds suggest that singlet states associated with both the ^1BL and the $[\text{Ir}(\text{C}^{\wedge}\text{N})_2]^+$ nodes (^1LC and $^1\text{MLCT}$) can be populated, the former being the most evident when $\text{BL} = \text{EDI}$, the latter when $\text{C}^{\wedge}\text{N} = \text{bt}$ and piq . Though we cannot specify the exact internal conversion/intersystem crossing pathways that populate the emissive T_1 state, we do observe that the excitation spectra (Figures S41–S49 of Supporting Information) overlay well with the UV–vis absorption, indicating that the same T_1 state is populated no matter which singlet state is excited. In complexes with $\text{C}^{\wedge}\text{N} = \text{bt}$ and piq , along with **Ir1**, the T_1 state is a $^3\text{LC}/^3\text{MLCT}$ state centered on the $[\text{Ir}(\text{C}^{\wedge}\text{N})_2]^+$ nodes (top diagram of Figure 5). The energy of this state depends on the cyclometalating ligand, as has been documented in numerous other studies. Consistent with this, in all of these compounds, both the room-temperature and 77 K photoluminescence (Figure 2) strongly resemble many other mononuclear $[\text{Ir}(\text{C}^{\wedge}\text{N})_2(\text{CNAr})_2]^+$ complexes. The energy of the bridging-ligand triplet state in these compounds, ^3BL , depends on which BL is used, but in all cases, it is higher in energy than $^3\text{LC}/^3\text{MLCT}$ and does not contribute to the observed luminescence. That said, the abnormally low quantum yield in some compounds, particularly evident in **Ir1** and to a lesser extent in $\text{C}^{\wedge}\text{N} = \text{bt}$ complexes **Ir5** and **Ir8**, suggests that the weakly luminescent ^3BL state may be thermally accessible in these compounds at room temperature, which results in a decrease in the quantum yield. In contrast, for the $\text{C}^{\wedge}\text{N} = \text{piq}$ complexes, **Ir3**, **Ir6**, and **Ir9**, there is larger energy separation between the $^3\text{LC}/^3\text{MLCT}$ and ^3BL states, and in these compounds, the quantum yields are not dependent on the bridge. In **Ir4** and **Ir7**, the ^3BL state is lowest in energy, and weak phosphorescence originates from that state (bottom diagram of Figure 5). The phosphorescence in these compounds strongly resembles that of the aromatic hydrocarbon core, though red-shifted as a result of the isocyano groups. In these compounds, it is likely that the $\text{C}^{\wedge}\text{N}$ -centered $^3\text{LC}/^3\text{MLCT}$ state can be initially populated following intersystem crossing, but internal conversion to the ^3BL state occurs prior to luminescence.

CONCLUSIONS

In this work, we described a synthetic strategy using coordination-driven self-assembly to synthesize nine new phosphorescent iridium(III) M_4L_4 coordination cages with cyclometalated iridium ($[\text{Ir}(\text{C}^{\wedge}\text{N})_2]^+$) nodes. Self-assembly of bis-cyclometalated iridium complexes is rare, in large part due to the substitutional inertness of Ir(III), and here, we introduce linear aryl diisocyanide BLs, whose strong coordination ability facilitates rapid, facile, and selective assembly of the M_4L_4 squares. Reactions proceed under milder conditions (ca. 40 °C) and with shorter reaction times (5 h) than that is often required for Ir(III) self-assembly, indicating some synthetic advantages of using isocyanide-based ligands in self-assembly. The photophysical consequences of the isocyanide BLs are also apparent. For most compounds, the photoluminescence strongly resembles that of mononuclear isocyanide-bound cyclometalated iridium complexes, originating from the $[\text{Ir}(\text{C}^{\wedge}\text{N})_2]^+$ node. In these cases, the electronic consequences of the isocyanide are apparent, with a sharper vibronic structure, bluer-shifted peak maxima, and longer lifetimes than that is typically observed in iridium cyclometalates. However, in two of the compounds with extended π -conjugation on the aryl diisocyanide, the BL is directly

involved in the photophysics, with the lowest-energy triplet state localizing on the BL and producing weak luminescence from that state. This work shows that isocyanide-based BLs offer advantages in the synthetic chemistry of self-assembled polynuclear cyclometalated iridium complexes and can also influence the photophysics, motivating continued pursuit of isocyanide-bridged cyclometalated iridium cages with diversified structures and exploration of their applications in optoelectronics, sensing, and photochemistry.

EXPERIMENTAL SECTION

Materials. All reagents and solvents were commercially obtained and used as received, unless otherwise noted. Reactions were performed in an open atmosphere fume hood, unless otherwise stated. BPDI and EDI were prepared using known literature procedures for converting aniline precursors into isocyanides,^{34,47} and PDI was commercially obtained from Acros Organics and used as obtained.

Physical Methods. ^1H NMR spectra were recorded at room temperature using a JEOL ECA-500 and JEOL ECA-600 spectrometer with frequencies of 500 and 600 MHz, respectively. All NMR data were processed using Delta software version 5.3.1 and presented with MestReNova software version 14.1.2-25024. Mass spectra were acquired with a Bruker Daltonics Solarix 12T Fourier Transform Ion Cyclotron Resonance Mass Spectrometer and analyzed using Bruker Compass DataAnalysis 4.2 software. ESI-MS results given in the experimental section are monoisotopic masses, and full experimental and simulated traces are presented in Figures S20–S28 in Supporting Information. UV–vis spectra were collected using an Agilent Carey 8454 UV–vis spectrophotometer. Emission spectra were collected using a Horiba FluoroMax-4 spectrofluorometer. Excitation spectra were collected in 1 cm quartz cuvettes using the Horiba FluoroMax-4 spectrofluorometer. Each cuvette was prepared in a glovebox with deoxygenated dichloromethane. The excitation spectrum was collected by monitoring at a fixed detection wavelength (corresponding to the emission maximum of each sample) while varying the excitation wavelength. Phosphorescence lifetimes were measured on a Horiba DeltaFlex Lifetime System, using 330 nm excitation and appropriate long-pass filters. All room-temperature photophysical measurements were carried out in 1 cm quartz cuvettes prepared in a glovebox with deaerated dichloromethane to exclude oxygen from measurements. Low-temperature measurements were performed with custom electron paramagnetic resonance tubes with high vacuum Teflon valve seals, in a 3:1 mixture of toluene to dichloromethane in a finger Dewar cooled to 77 K with liquid nitrogen. Emission quantum yields were determined relative to a standard of tetraphenylporphyrin in toluene ($\Phi_{\text{F}} = 0.11$).

General Procedure for Synthesis of $[\text{Ir}(\text{C}^{\wedge}\text{N})_2(\text{NCMe})_2]\text{PF}_6$. $[\text{Ir}(\text{C}^{\wedge}\text{N})_2(\mu\text{-Cl})_2]$ (1.0 equiv) and silver hexafluorophosphate (2.5 equiv) were dissolved in dry acetonitrile in a glovebox. After stirring for 2 h at room temperature, the mixture was removed from the glovebox and refluxed for an additional 2 h at 60 °C. After cooling to room temperature, the mixture was filtered through Celite to collect AgCl formed in the reaction. The solvent was then removed under vacuum. The product was dissolved in the minimum amount of CH_2Cl_2 and precipitated with diethyl ether. The solid was then filtered, washed with excess diethyl ether, and dried under vacuum with gentle heating at 30 °C for 24 h.

General Procedure for Synthesis of $[\text{Ir}(\text{C}^{\wedge}\text{N})_2(\mu\text{-BL})_4](\text{PF}_6)_4$ Complexes (Scheme 1). Complexes **Ir1–Ir9** were synthesized by treating the respective $[\text{Ir}(\text{C}^{\wedge}\text{N})_2(\text{NCMe})_2]\text{PF}_6$ complex (1.0 equiv) with the linear diisocyanide BL (1.0 equiv) in 10–30 mL of dichloromethane, heating at 40 °C in a Schlenk flask under a N_2 atmosphere for 5 h. After cooling to room temperature, the solvent was then removed under vacuum. The product was dissolved in the minimum amount of CH_2Cl_2 and precipitated with diethyl ether. The solid was then filtered and washed with excess diethyl ether and finally dried under vacuum with gentle heating at 30 °C for 24 h.

Synthesis of [Ir(ppy)₂(μ-PDI)]₄(PF₆)₄ (Ir1). Prepared by the general procedure above using [Ir(ppy)₂(NCMe)₂]₂PF₆ (63 mg) and PDI (12 mg). Yield: 39 mg, 58%. ¹H NMR (600 MHz, CD₃CN): δ = 9.16 (s, 8H, ppy, Ar H), 8.13 (s, 16H, ppy, Ar H), 7.75 (s, 8H, ppy, Ar H), 7.59–7.32 (m, 24H, ppy/PDI, Ar H), 7.01 (s, 8H, ppy, Ar H), 6.88 (s, 8H, ppy, Ar H), 6.11 (s, 8H, ppy, Ar H). HRMS (ESI) *m/z*: [M – 2PF₆]²⁺ calcd, 1403.22708; found, 1403.26009; [M – 3PF₆]³⁺ calcd, 887.16314; found, 887.17682. FT-IR (cm⁻¹): 2131 ($\tilde{\nu}_{\text{CN}}$), 2167 (sh) ($\tilde{\nu}_{\text{CN}}$).

Synthesis of [Ir(bt)₂(μ-PDI)]₄(PF₆)₄ (Ir2). Prepared by the general procedure using [Ir(bt)₂(NCMe)₂]₂PF₆ (59 mg) and PDI (9 mg). Yield: 33 mg, 53%. ¹H NMR (600 MHz, CD₃CN): δ = 8.39–8.13 (m, 16H, bt, Ar H), 7.90–7.56 (m, 24H, bt, Ar H), 7.52–7.24 (m, 16H, PDI, Ar H), 7.04 (s, 8H, bt, Ar H), 6.89 (s, 8H, bt, Ar H), 6.17 (s, 8H, bt, Ar H). HRMS (ESI) *m/z*: [M – 2PF₆]²⁺ calcd, 1627.11536; found, 1627.16055; [M – 3PF₆]³⁺ calcd, 1036.42110; found, 1036.44181. FT-IR (cm⁻¹): 2126 ($\tilde{\nu}_{\text{CN}}$), 2171 (sh) ($\tilde{\nu}_{\text{CN}}$).

Synthesis of [Ir(piq)₂(μ-PDI)]₄(PF₆)₄ (Ir3). Prepared by the general procedure using [Ir(piq)₂(NCMe)₂]₂PF₆ (37 mg) and PDI (6 mg). Yield: 20 mg, 51%. ¹H NMR (500 MHz, CD₃CN): δ = 9.04 (s, 8H, piq, Ar H), 8.92 (s, 8H, piq, Ar H), 8.28 (s, 8H, piq, Ar H), 8.14 (s, 8H, piq, Ar H), 8.00–7.71 (m, 24H, piq, Ar H), 7.64–7.24 (m, 24H, piq/PDI, Ar H), 7.07 (s, 8H, piq, Ar H), 6.83 (s, 8H, piq, Ar H), 6.11 (s, 8H, piq, Ar H). HRMS (ESI) *m/z*: [M – 2PF₆]²⁺ calcd, 1603.28968; found, 1603.30502; [M – 3PF₆]³⁺ calcd, 1020.53821; found, 1020.55971. FT-IR (cm⁻¹): 2127 ($\tilde{\nu}_{\text{CN}}$), 2170 (sh) ($\tilde{\nu}_{\text{CN}}$).

Synthesis of [Ir(ppy)₂(μ-BPDI)]₄(PF₆)₄ (Ir4). Prepared by the general procedure using [Ir(ppy)₂(NCMe)₂]₂PF₆ (30 mg) and BPDI (8 mg). Yield: 16 mg, 46%. ¹H NMR (500 MHz, CD₃CN): δ = 9.26 (s, 8H, ppy, Ar H), 8.14 (d, J = 24.8 Hz, 16H, ppy, Ar H), 7.79 (s, 8H, ppy, Ar H), 7.73–7.63 (m, 16H, BPDI, Ar H), 7.61–7.38 (m, 24H, ppy/BPDI, Ar H), 7.02 (d, J = 7.3 Hz, 8H, ppy, Ar H), 6.92 (s, 8H, ppy, Ar H), 6.19 (d, J = 7.7 Hz, 8H, ppy, Ar H). HRMS (ESI) *m/z*: [M – 2PF₆]²⁺ calcd, 1555.28968; found, 1555.32318; [M – 3PF₆]³⁺ calcd, 988.53821; found, 988.55519. FT-IR (cm⁻¹): 2131 ($\tilde{\nu}_{\text{CN}}$), 2162 (sh) ($\tilde{\nu}_{\text{CN}}$).

Synthesis of [Ir(bt)₂(μ-BPDI)]₄(PF₆)₄ (Ir5). Prepared by the general procedure using [Ir(bt)₂(NCMe)₂]₂PF₆ (30 mg) and BPDI (8 mg). Yield: 14 mg, 40%. ¹H NMR (500 MHz, CD₃CN): δ = 8.42 (d, J = 8.2 Hz, 8H, bt, Ar H), 8.23 (s, 8H, bt, Ar H), 7.86 (d, J = 8.6 Hz, 8H, bt, Ar H), 7.75 (s, 8H, bt, Ar H), 7.70–7.52 (m, 24H, bt/BPDI, Ar H), 7.41–7.30 (m, 16H, BPDI, Ar H), 7.07 (t, J = 7.1 Hz, 8H, bt, Ar H), 6.93 (t, J = 7.7 Hz, 8H, bt, Ar H), 6.25 (d, J = 7.6 Hz, 8H, bt, Ar H). HRMS (ESI) *m/z*: [M – 2PF₆]²⁺ calcd, 1779.17796; found, 1779.20868; [M – 3PF₆]³⁺ calcd, 1137.79707; found, 1137.81026. FT-IR (cm⁻¹): 2144 ($\tilde{\nu}_{\text{CN}}$), 2170 (sh) ($\tilde{\nu}_{\text{CN}}$).

Synthesis of [Ir(piq)₂(μ-BPDI)]₄(PF₆)₄ (Ir6). Prepared by the general procedure using [Ir(piq)₂(NCMe)₂]₂PF₆ (24 mg) and BPDI (6 mg). Yield: 21 mg, 78%. ¹H NMR (500 MHz, CD₃CN): δ = 9.16 (s, 8H, piq, Ar H), 8.97 (d, J = 7.3 Hz, 8H, piq, Ar H), 8.32 (d, J = 9.5 Hz, 8H, piq, Ar H), 8.22–8.09 (m, 8H, piq, Ar H), 8.00–7.76 (m, 24H, piq, Ar H), 7.72–7.53 (m, 16H, BPDI, Ar H), 7.53–7.32 (m, 16H, BPDI, Ar H), 7.10 (d, J = 9.0 Hz, 8H, piq, Ar H), 6.86 (s, 8H, piq, Ar H), 6.19 (d, J = 7.6 Hz, 8H, piq, Ar H). HRMS (ESI) *m/z*: [M – 2PF₆]²⁺ calcd, 1755.35228; found, 1755.36982; [M – 3PF₆]³⁺ calcd, 1121.91328; found, 1121.92311. FT-IR (cm⁻¹): 2140 ($\tilde{\nu}_{\text{CN}}$), 2166 (sh) ($\tilde{\nu}_{\text{CN}}$).

Synthesis of [Ir(ppy)₂(μ-EDI)]₄(PF₆)₄ (Ir7). Prepared by the general procedure using [Ir(ppy)₂(NCMe)₂]₂PF₆ (28 mg) and EDI (8 mg). Yield: 27 mg, 83%. ¹H NMR (500 MHz, CD₃CN): δ = 9.24 (s, 8H ppy, Ar H), 8.19–8.09 (m, 16H ppy, Ar H), 7.79 (d, J = 8.0 Hz, 8H ppy, Ar H), 7.64–7.53 (m, 16H EDI, Ar H), 7.47–7.35 (m, 24H ppy/EDI, Ar H), 7.03 (t, J = 7.7 Hz, 8H ppy, Ar H), 6.92 (t, J = 7.4 Hz, 8H ppy, Ar H), 6.18 (d, J = 8.0 Hz, 8H ppy, Ar H). HRMS (ESI) *m/z*: [M – 3PF₆]³⁺ calcd, 1020.53821; found, 1020.58226. FT-IR (cm⁻¹): 2136 ($\tilde{\nu}_{\text{CN}}$), 2165 (sh) ($\tilde{\nu}_{\text{CN}}$).

Synthesis of [Ir(bt)₂(μ-EDI)]₄(PF₆)₄ (Ir8). Prepared by the general procedure using [Ir(bt)₂(NCMe)₂]₂PF₆ (24 mg) and EDI (6 mg). Yield: 14 mg, 48%. ¹H NMR (500 MHz, CD₃CN): δ = 8.39 (d, J = 8.7 Hz, 8H, bt, Ar H), 8.23 (q, J = 7.9, 6.0 Hz, 8H, bt, Ar H), 7.86

(q, J = 9.0, 8.2 Hz, 8H, bt, Ar H), 7.76 (t, J = 7.6 Hz, 8H, bt, Ar H), 7.71–7.62 (m, 8H, bt, Ar H), 7.59–7.49 (m, 16H, EDI, Ar H), 7.45–7.26 (m, 16H, EDI, Ar H), 7.08 (dd, J = 9.9, 5.6 Hz, 8H, bt, Ar H), 6.92 (q, J = 7.4 Hz, 8H, bt, Ar H), 6.24 (d, J = 7.4 Hz, 8H, bt, Ar H). HRMS (ESI) *m/z*: [M – 3PF₆]³⁺ calcd, 1169.79707; found, 1169.85281. FT-IR (cm⁻¹): 2139 ($\tilde{\nu}_{\text{CN}}$), 2168 (sh) ($\tilde{\nu}_{\text{CN}}$).

Synthesis of [Ir₄(piq)₈(μ-EDI)]₄(PF₆)₄ (Ir9). Prepared by the general procedure using [Ir(piq)₂(NCMe)₂]₂PF₆ (29 mg) and EDI (8 mg). Yield: 22 mg, 63%. ¹H NMR (500 MHz, CD₃CN): δ = 9.14 (t, J = 6.0 Hz, 8H, piq, Ar H), 8.97 (d, J = 8.7 Hz, 8H, piq, Ar H), 8.33 (d, J = 7.7 Hz, 8H, piq, Ar H), 8.18 (t, J = 6.4 Hz, 8H, piq, Ar H), 8.01–7.77 (m, 24H, piq, Ar H), 7.62–7.30 (m, 32H, EDI, Ar H), 7.11 (t, J = 6.6 Hz, 8H, piq, Ar H), 6.86 (t, J = 7.7 Hz, 8H, piq, Ar H), 6.19 (q, J = 6.9 Hz, 8H, piq, Ar H). HRMS (ESI) *m/z*: [M – 3PF₆]³⁺ calcd, 1153.91328; found, 1153.96859. FT-IR (cm⁻¹): 2132 ($\tilde{\nu}_{\text{CN}}$), 2155 (sh) ($\tilde{\nu}_{\text{CN}}$).

General Procedure for Synthesis of Diisocyanide Ligands.

The linear BLs were synthesized via a known two-step procedure for converting aniline precursors into isocyanides.⁴⁷ The dianiline precursor is formylated using acetic formic anhydride, prepared in situ through reaction of acetic anhydride and formic acid. Formic acid (32 equiv) and acetic anhydride (33 equiv) are allowed to stir together at 0 °C for 30 min. Afterward, the mixture is allowed to reflux at 60 °C for 3 h. After cooling to room temperature the prepared acetic formic anhydride is added to the aniline precursor (1.0 equiv) dissolved in tetrahydrofuran and allowed to stir overnight. The solvent was then removed under vacuum, yielding a white or tan solid. The solid was collected in a vial and dried under vacuum with gentle heating at 30 °C for 24 h. The resulting formylamide is then dehydrated with phosphoryl chloride and diisopropyl amine to yield the linear diisocyanides. Without further purification, the formylamide (1.0 equiv) from the first step was added to dichloromethane forming a suspension. Diisopropylamine (7.0 equiv) and phosphorous oxychloride (2.8 equiv) were added to the suspension. The mixture was cooled to 0 °C and allowed to stir for 30 min, followed by 8 h of stirring at room temperature. The reaction was quenched by adding saturated aqueous Na₂CO₃ and stirred for 24 h. A biphasic extraction with dichloromethane was performed with two brine washes. The organic layer was dried over MgSO₄, then filtered, and the solvent was removed under vacuum yielding the crude product. The product was purified by performing a silica flash column eluted with dichloromethane, yielding the pure diisocyanide.

Synthesis of BPDI. Prepared by general procedure using benzidine (513 mg, 28 mmol, 1.0 equiv) with acetic anhydride (9 mL, 92 mmol, 33 equiv) and formic acid (3.5 mL, 90 mmol, 32 equiv). Yield: 524 mg, 78%. *N,N'*-[1,1'-biphenyl]-4,4'-diyl-bis(formamide) (227 mg, 0.94 mmol, 1.0 equiv) with diisopropylamine (0.5 mL, 62 mmol, 6.0 equiv) and phosphorous oxychloride (0.4 mL, 38 mmol, 4.0 equiv). Yield: 82 mg, 38%. ¹H NMR (600 MHz, CD₂Cl₂): δ = 7.59 (d, J = 8.3 Hz, 4H), 7.46 (d, J = 8.2 Hz, 4H). ¹³C{¹H} NMR (151 MHz, CD₂Cl₂): δ (ppm) 165.7, 140.5, 128.2, 127.1, 126.4. FT-IR (cm⁻¹): 2124 ($\tilde{\nu}_{\text{CN}}$).

Synthesis of EDI. Prepared by general procedure of diisocyanide ligands using 4,4'-ethyne-1,2-diyl-dianiline (500 mg, 2.4 mmol, 1.0 equiv) with acetic anhydride (8 mL, 79 mmol, 33 equiv) and formic acid (3 mL, 76 mmol, 32 equiv). Yield: 568 mg, 89%. 4,4'-Ethyne-1,2-diyl-bis(formamide) (268 mg, 1.0 mmol, 1.0 equiv) with diisopropylamine (0.5 mL, 71 mmol, 7.0 equiv) and phosphorous oxychloride (0.3 mL, 28 mmol, 2.8 equiv). Yield: 85 mg, 36%. ¹H NMR (600 MHz, CD₂Cl₂): δ = 7.55 (d, J = 8.3 Hz, 4H), 7.37 (d, J = 8.2 Hz, 4H). ¹³C{¹H} NMR (151 MHz, CD₂Cl₂): δ (ppm) 166.5, 132.7, 126.7, 126.2, 123.9, 90.2. FT-IR (cm⁻¹): 2125 ($\tilde{\nu}_{\text{CN}}$).

■ ASSOCIATED CONTENT

Supporting Information

The Supporting Information is available free of charge at <https://pubs.acs.org/doi/10.1021/acs.inorgchem.1c00312>.

NMR spectra, mass spectrometry data, infrared spectra, and additional photophysical data (PDF)

AUTHOR INFORMATION

Corresponding Author

Thomas S. Teets – Department of Chemistry, University of Houston, Houston, Texas 77204-5003, United States;

orcid.org/0000-0002-7471-8467; Email: tteets@uh.edu

Authors

Morris E. Olumba – Department of Chemistry, University of Houston, Houston, Texas 77204-5003, United States

Hanah Na – Department of Chemistry, University of Houston, Houston, Texas 77204-5003, United States

Alan E. Friedman – Department of Materials, Design, and Innovation, University at Buffalo, The State University of New York, Buffalo, New York 14260, United States;

orcid.org/0000-0002-4764-8168

Complete contact information is available at:

<https://pubs.acs.org/10.1021/acs.inorgchem.1c00312>

Notes

The authors declare no competing financial interest.

ACKNOWLEDGMENTS

The authors acknowledge the Army Research Lab (Cooperative Agreement W911NF1920196) and the Welch Foundation (grant no E-1887) for funding.

REFERENCES

- Balzani, V.; Juris, A.; Venturi, M.; Campagna, S.; Serroni, S. Luminescent and Redox-Active Polynuclear Transition Metal Complexes†. *Chem. Rev.* **1996**, *96*, 759–833.
- Martir, D. R.; Pizzolante, A.; Escudero, D.; Jacquemin, D.; Warriner, S. L.; Zysman-Colman, E. Photoinduced Energy and Electron Transfer Between a Photoactive Cage Based on a Thermally Activate Delayed Fluorescence Ligand and Encapsulated Fluorescent Dyes. *ACS Appl. Energy Mater.* **2018**, *1*, 2971–2978.
- Shen, C.; Kennedy, A. D. W.; Donald, W. A.; Torres, A. M.; Price, W. S.; Beves, J. E. Self-Assembled Supramolecular Cages Containing Dinuclear Ruthenium(II) Polypyridyl Complexes. *Inorg. Chim. Acta.* **2017**, *458*, 122–128.
- Yan, X.; Wang, H.; Hauke, C. E.; Cook, T. R.; Wang, M.; Saha, M. L.; Zhou, Z.; Zhang, M.; Li, X.; Huang, F.; Stang, P. J. A Suite of Tetraphenylethylene-Based Discrete Organoplatinum(II) Metallacycles: Controllable Structure and Stoichiometry, Aggregation-Induced Emission, and Nitroaromatics Sensing. *J. Am. Chem. Soc.* **2015**, *137*, 15276–15286.
- Yan, X.; Cook, T. R.; Wang, P.; Huang, F.; Stang, P. J. Highly Emissive Platinum(II) Metallacycles. *Nat. Chem.* **2015**, *7*, 342–348.
- Gupta, D.; Sathiyendiran, M. Rhenium-Carbonyl-Based Supramolecular Coordination Complexes: Synthesis, Structure and Properties. *ChemistrySelect* **2018**, *3*, 7439–7458.
- Cullen, W.; Takezawa, H.; Fujita, M. Demethylation of Cyclopropanes via Photoinduced Guest-to-Host Electron Transfer in an M₆L₄ Cage. *Angew. Chem., Int. Ed.* **2019**, *58*, 9171–9173.
- Chakrabarty, R.; Mukherjee, P. S.; Stang, P. J. Supramolecular Coordination: Self-Assembly of Finite Two- and Three-Dimensional Ensembles. *Chem. Rev.* **2011**, *111*, 6810–6918.
- Komine, S.; Takahashi, S.; Kojima, T.; Sato, H.; Hiraoka, S. Self-Assembly Processes of Octahedron-Shaped Pd₆L₄ Cages. *J. Am. Chem. Soc.* **2019**, *141*, 3178–3186.
- Fang, Y.; Powell, J. A.; Li, E.; Wang, Q.; Perry, Z.; Kirchon, A.; Yang, X.; Xiao, Z.; Zhu, C.; Zhang, L.; Huang, F.; Zhou, H.-C. Catalytic Reactions within the Cavity of Coordination Cages. *Chem. Soc. Rev.* **2019**, *48*, 4707–4730.
- Baranoff, E.; Orselli, E.; Allouche, L.; Di Censo, D.; Scopelliti, R.; Grätzel, M.; Nazeeruddin, M. K. A Bright Tetranuclear Iridium(III) Complex. *Chem. Commun.* **2011**, *47*, 2799–2801.
- Chepelin, O.; Ujma, J.; Wu, X.; Slawin, A. M. Z.; Pitak, M. B.; Coles, S. J.; Michel, J.; Jones, A. C.; Barran, P. E.; Lusby, P. J. Luminescent, Enantiopure, Phenylatopyridine Iridium-Based Coordination Capsules. *J. Am. Chem. Soc.* **2012**, *134*, 19334–19337.
- Oldknow, S.; Martir, D. R.; Pritchard, V. E.; Blitz, M. A.; Fishwick, C. W. G.; Zysman-Colman, E.; Hardie, M. J. Structure-Switching M₃L₂ Ir(III) Coordination Cages with Photo-Isomerising Azo-Aromatic Linkers. *Chem. Sci.* **2018**, *9*, 8150–8159.
- Shiu, L. C.; Chang, B. R.; Hsiao, M. C. S.; Sie, W. S.; Wu, M. L.; Huang, L. X.; Wang, C. M.; Lee, G. H.; Chang, I. J.; Su, H. C.; Shiu, K. B. Alkyl-Spacer Enhancement in Performance of Light-Emitting Electrochemical Cells. *Eur. J. Inorg. Chem.* **2020**, *2020*, 3517–3526.
- Zysman-colman, E. *Iridium(III) in Optoelectronic and Photonics Applications*; John Wiley & Sons, 2017.
- Yu, G.; Cook, T. R.; Li, Y.; Yan, X.; Wu, D.; Shao, L.; Shen, J.; Tang, G.; Huang, F.; Chen, X.; Stang, P. J. Tetraphenylethylene-Based Highly Emissive Metallacycle as a Component of Theranostic Supramolecular Nanoparticles. *Proc. Natl. Acad. Sci.* **2016**, *113*, 13720–13725.
- Juris, A.; Balzani, V.; Barigelletti, F.; Campagna, S.; Belser, P.; von Zelewsky, A. Ru(II) Polypyridine Complexes: Photophysics, Photochemistry, Electrochemistry, and Chemiluminescence. *Coord. Chem. Rev.* **1988**, *84*, 85–277.
- Sauvage, J. P.; Collin, J. P.; Chambron, J. C.; Guillerez, S.; Coudret, C.; Balzani, V.; Barigelletti, F.; De Cola, L.; Flamigni, L. Ruthenium(II) and Osmium(II) Bis(Terpyridine) Complexes in Covalently-Linked Multicomponent Systems: Synthesis, Electrochemical Behavior, Absorption Spectra, and Photochemical and Photophysical Properties. *Chem. Rev.* **1994**, *94*, 993–1019.
- Han, Y.-F.; Fei, Y.; Jin, G.-X. Self-Assembled Half-Sandwich Ir, Rh-Based Organometallic Molecular Boxes for Reversible Trapping of Halocarbon Molecules. *Dalton Trans.* **2010**, *39*, 3976–3984.
- Zhang, W.-Y.; Han, Y.-F.; Weng, L.-H.; Jin, G.-X. Synthesis, Characterization, and Properties of Half-Sandwich Iridium/Rhodium-Based Metallarectangles. *Organometallics* **2014**, *33*, 3091–3095.
- Oshio, H.; Tamada, O.; Onodera, H.; Ito, T.; Ikoma, T.; Tero-Kubota, S. Cyanide-Bridged Iron–Copper Molecular Squares with Doublet and Quintet Spin Ground States. *Inorg. Chem.* **1999**, *38*, 5686–5689.
- Zueva, E. M.; Ryabikh, E. R.; Kuznetsov, A. M.; Borshch, S. A. Spin Crossover in Tetranuclear Cyanide-Bridged Iron(II) Square Complexes: A Theoretical Study. *Inorg. Chem.* **2011**, *50*, 1905–1913.
- Nihei, M.; Sekine, Y.; Suganami, N.; Nakazawa, K.; Nakao, A.; Nakao, H.; Murakami, Y.; Oshio, H. Controlled Intramolecular Electron Transfers in Cyanide-Bridged Molecular Squares by Chemical Modifications and External Stimuli. *J. Am. Chem. Soc.* **2011**, *133*, 3592–3600.
- Lin, J.-L.; Tsai, C.-N.; Huang, S.-Y.; Endicott, J. F.; Chen, Y.-J.; Chen, H.-Y. Nearest- and Next-Nearest-Neighbor Ru(II)/Ru(III) Electronic Coupling in Cyanide-Bridged Tetra-Ruthenium Square Complexes. *Inorg. Chem.* **2011**, *50*, 8274–8280.
- Chen, J.; Calvet, L. C.; Reed, M. A.; Carr, D. W.; Grubisha, D. S.; Bennett, D. W. Electronic Transport through Metal–1,4-Phenylene Diisocyanide–Metal Junctions. *Chem. Phys. Lett.* **1999**, *313*, 741–748.
- Hong, S.; Reifengerger, R.; Tian, W.; Datta, S.; Henderson, J. I.; Kubiak, C. P. Molecular Conductance Spectroscopy of Conjugated, Phenyl-Based Molecules on Au(111): The Effect of End Groups on Molecular Conduction. *Superlattices Microstruct.* **2000**, *28*, 289–303.
- Shen, W.; Lin, X.; Jiang, C.; Li, C.; Lin, H.; Huang, J.; Wang, S.; Liu, G.; Yan, X.; Zhong, Q.; Ren, B. Reliable Quantitative SERS Analysis Facilitated by Core-Shell Nanoparticles with Embedded Internal Standards. *Angew. Chem., Int. Ed.* **2015**, *54*, 7308–7312.

- (28) Farrell, J. R.; Mirkin, C. A.; Guzei, I. A.; Liable-Sands, L. M.; Rheingold, A. L. The Weak-Link Approach to the Synthesis of Inorganic Macrocycles. *Angew. Chem., Int. Ed.* **1998**, *37*, 465–467.
- (29) Coco, S.; Cordovilla, C.; Espinet, P.; Martín-Alvarez, J.; Muñoz, P. Dinuclear Gold(I) Isocyanide Complexes with Luminescent Properties, and Displaying Thermotropic Liquid Crystalline Behavior. *Inorg. Chem.* **2006**, *45*, 10180–10187.
- (30) Ito, H.; Saito, T.; Oshima, N.; Kitamura, N.; Ishizaka, S.; Hinatsu, Y.; Wakeshima, M.; Kato, M.; Tsuge, K.; Sawamura, M. Reversible Mechanochromic Luminescence of $[(C_6F_5Au)_2(\mu-1,4\text{-Diisocyanobenzene})]$. *J. Am. Chem. Soc.* **2008**, *130*, 10044–10045.
- (31) Lin, P.-C.; Chen, H.-Y.; Chen, P.-Y.; Chiang, M.-H.; Chiang, M. Y.; Kuo, T.-S.; Hsu, S. C. N. Self-Assembly and Redox Modulation of the Cavity Size of an Unusual Rectangular Iron Thiolate Aryldiisocyanide Metallocyclophane. *Inorg. Chem.* **2011**, *50*, 10825–10834.
- (32) Qin, L.; Guan, X.; Yang, C.; Huang, J.-S.; Che, C.-M. Near-Infrared Phosphorescent Supramolecular Alkyl/Aryl-Iridium Porphyrin Assemblies by Axial Coordination. *Chem. —Eur. J.* **2018**, *24*, 14400–14408.
- (33) Hauke, C. E.; Oldacre, A. N.; Fulong, C. R. P.; Friedman, A. E.; Cook, T. R. Coordination-Driven Self-Assembly of Ruthenium Polypyridyl Nodes Resulting in Emergent Photophysical and Electrochemical Properties. *Inorg. Chem.* **2018**, *57*, 3587–3595.
- (34) Sattler, W.; Henling, L. M.; Winkler, J. R.; Gray, H. B. Bespoke Photoreductants: Tungsten Arylisocyanides. *J. Am. Chem. Soc.* **2015**, *137*, 1198–1205.
- (35) Maity, A.; Le, L. Q.; Zhu, Z.; Bao, J.; Teets, T. S. Steric and Electronic Influence of Aryl Isocyanides on the Properties of Iridium(III) Cyclometalates. *Inorg. Chem.* **2016**, *55*, 2299–2308.
- (36) Na, H.; Maity, A.; Teets, T. S. Bis-Cyclometalated Iridium Complexes with Electronically Modified Aryl Isocyanide Ancillary Ligands. *Dalton Trans.* **2017**, *46*, 5008–5016.
- (37) Cañada, L. M.; Kölling, J.; Teets, T. S. Blue-Phosphorescent Bis-Cyclometalated Iridium Complexes with Aryl Isocyanide Ancillary Ligands. *Polyhedron* **2020**, *178*, 114332.
- (38) Nonoyama, M. Benzo[h]quinolin-10-yl-N Iridium(III) Complexes. *Bull. Chem. Soc. Jpn.* **1974**, *47*, 767–768.
- (39) Shik Chin, C.; Eum, M.-S.; Yi Kim, S.; Kim, C.; Kwon Kang, S. Blue-Light-Emitting Complexes: Cationic (2-Phenylpyridinato)-Iridium(III) Complexes with Strong-Field Ancillary Ligands. *Eur. J. Inorg. Chem.* **2007**, *2007*, 372–375.
- (40) Pritchard, V. E.; Rota Martir, D.; Zysman-Colman, E.; Hardie, M. J. Multimetallic and Mixed Environment Iridium(III) Complexes: A Modular Approach to Luminescence Tuning Using a Host Platform. *Chem. —Eur. J.* **2017**, *23*, 8839–8849.
- (41) Tinker, L. L.; McDaniel, N. D.; Cline, E. D.; Bernhard, S. Heteroleptic Cyclometalated Iridium(III) Complexes. *Inorg. Synth.* **2010**, *35*, 168–173.
- (42) Na, H.; Song, M.; Teets, T. S. Facile Synthesis of Luminescent Ir–Pt–Ir Trimetallic Complexes. *Chem. —Eur. J.* **2019**, *25*, 4833–4842.
- (43) Yersin, H.; Rausch, A. F.; Czerwieniec, R.; Hofbeck, T.; Fischer, T. The Triplet State of Organo-Transition Metal Compounds. Triplet Harvesting and Singlet Harvesting for Efficient OLEDs. *Coord. Chem. Rev.* **2011**, *255*, 2622–2652.
- (44) Fries, F.; Louis, M.; Scholz, R.; Gmelch, M.; Thomas, H.; Haft, A.; Reineke, S. Dissecting Tetra-*N*-Phenylbenzidine: Biphenyl as the Origin of Room Temperature Phosphorescence. *J. Phys. Chem. A* **2020**, *124*, 479–485.
- (45) Nagano, Y.; Ikoma, T.; Akiyama, K.; Tero-Kubota, S. Symmetry Switching of the Fluorescent Excited State in α,ω -Diphenylpolyynes. *J. Am. Chem. Soc.* **2003**, *125*, 14103–14112.
- (46) Favale, J. M.; Hauke, C. E.; Danilov, E. O.; Yarnell, J. E.; Castellano, F. N. Ligand-Triplet Migration in Iridium(III) Cyclometalates Featuring π -Conjugated Isocyanide Ligands. *Dalton Trans.* **2020**, *49*, 9995–10002.
- (47) Goldman, W.; Nasulewicz-Goldman, A. Synthesis and Antiproliferative Activity of Aromatic and Aliphatic Bis-

[Aminomethylidene(Bisphosphonic)] Acids. *Bioorg. Med. Chem. Lett.* **2014**, *24*, 3475–3479.